Supporting Information for

A Biodegradable and Recyclable Piezoelectric Sensor Based on Molecular Ferroelectric Embedded in a Bacterial Cellulose Hydrogel

Junling Lu[1†], Sanming Hu[2†], Wenru Li[1†], Xuefang Wang[1], Xiwei Mo[1], Xuetian Gong[1], Huan Liu[1], Wei Luo[1], Wen Dong[1], Chaotan Sima[1], Yaojin Wang[3], Guang Yang[2], Jing-Ting Luo[4], Shenglin Jiang[1], Zhijun Shi[2*], and Guangzu Zhang[1*]*

[1]School of Optical and Electronic Information, Engineering Research Center for Functional Ceramics MOE and Wuhan National Laboratory for Optoelectronics, Huazhong University of Science and Technology, Wuhan, Hubei, 430074, China

[2]College of Life Science and Technology, Huazhong University of Science and Technology, Wuhan, Hubei, 430074, China

[3]School of Materials Science and Engineering, Nanjing University of Science and Technology, Nanjing, Jiangsu, 210094, China

[4]Key Laboratory of Optoelectronic Devices and Systems of Education Ministry and Guangdong Province, College of Physics and Optoelectronic Engineering, Shenzhen University, Shenzhen 518060, China

*Corresponding Author.

E-mail: zhanggz@hust.edu.cn; jsl@hust.edu.cn; shizhijun@hust.edu.cn

Table S1. Comparison of performances of various molecular ferroelectrics.

Materials	T_c (°C)	d_{33} (pC N^{-1})	Advantages	Disadvantages	Ref.
$(TMFM)_x(TMCM)_{1-x}CdCl_3$ (TMFM, trimethylfluoromethyl ammonium; TMCM, trimethylchloromethyl ammonium, $0 \leq x \leq 1$)	95-125	1540	• Ultrahigh d_{33} • Moderate T_c	• Complicated synthesis method	S1
Diisopropylammonium Bromide	148	11	• Moderate T_c • Facile fabrication process	• Low d_{33}	S2
Guanidinium Perchlorate	181	11	• High T_c	• Low d_{33}	S3
Imidazolium Periodate	37	4	• Facile fabrication	• Low d_{33} • Low T_c	S4
4-(phenyldiazenyl)anilinium) D- and L-tartrate	205	7	• High T_c	• Low d_{33}	S5
(4-aminotetrahydropyran)$_2$PbBr$_4$	200	48	• High d_{33} • High T_c	• Ultrahigh coercive field, difficult to be poled	S6
N-methyl-*N*′-diazabicyclo[2.2.2]octonium) -ammonium triiodide	175	14	• High T_c	• Low d_{33}	S7
N,*N*-dimethylallylammonium $CdCl_3$	66	41	• High d_{33}	• Low T_c	S8
Trimethylchloromethyl Ammonium Tribromocadmium(II)	73	139	• High d_{33} • High T_c	• Complicated synthesis method	S9
Imidazolium Perchlorate (this work)	100	41	• High d_{33} • High T_c • Facile fabrication		

Annotation: The piezoelectric effect is appeared in different ferroelectric materials including inorganic ferroelectrics (*e.g.*, single crystals and ceramics), ferroelectric polymers, and organic-inorganic hybrid molecular ferroelectrics. Inorganic ferroelectrics have superior piezoelectricity to their polymer counterpart, they are, however, hard and fragile, and thus hardly to be used for flexible devices. Ferroelectric polymers are featured with favorable flexible, however, its electric performance, *e.g.*, piezoelectric and pyroelectric properties, is relatively low. Moreover, even with facile preparation processes, for example, hot-pressing and solution casting, the fabrication of ferroelectric polymers with special structures or combining them with other structural or functional materials are still complicated. Compared to the conventional ferroelectric ceramics and polymers, many molecular ferroelectrics can be synthesized with very easy methods, for example, by evaporating saturated solutions. Among them, some molecular ferroelectrics, such as $ImClO_4$ we used in this work, possess higher piezoelectric coefficient (*e.g.*, d_{33}) than that of PVDF based polymers. Attached to flexible substrate, the hybrid material with molecular ferroelectrics also exhibit favorable flexibility. And thus, in this work, we chose molecular ferroelectric as the function element for the flexible sensors. Table S1, Supporting Information compared the piezoelectric coefficient (d_{33}), Curie temperature (T_c), and fabrication process of different typical molecular ferroelectrics. As listed in Table. S1, the d_{33} of diisopropylammonium bromide, guanidinium perchlorate, and imidazolium periodate is low. *N*,*N*-dimethylallylammonium $CdCl_3$ and trimethylchloromethyl ammonium tribromocadmium(II) have a high piezoelectricity, but the low Curie temperature causes the depolarization issue for the practical application. $(TMFM)_x(TMCM)_{1-x}CdCl_3$ (TMFM, trimethylfluoromethyl ammonium; TMCM, trimethylchloromethyl ammonium, $0 \leq x \leq 1$) and $(4\text{-aminotetrahydropyran})_2PbBr_4$ have high piezoelectric performance and Curie temperature, however, their fabrication process is incompatible with our BC-molecular ferroelectric hybrid strategy. Therefore, we chose $ImClO_4$ as the piezoelectric material in this work.

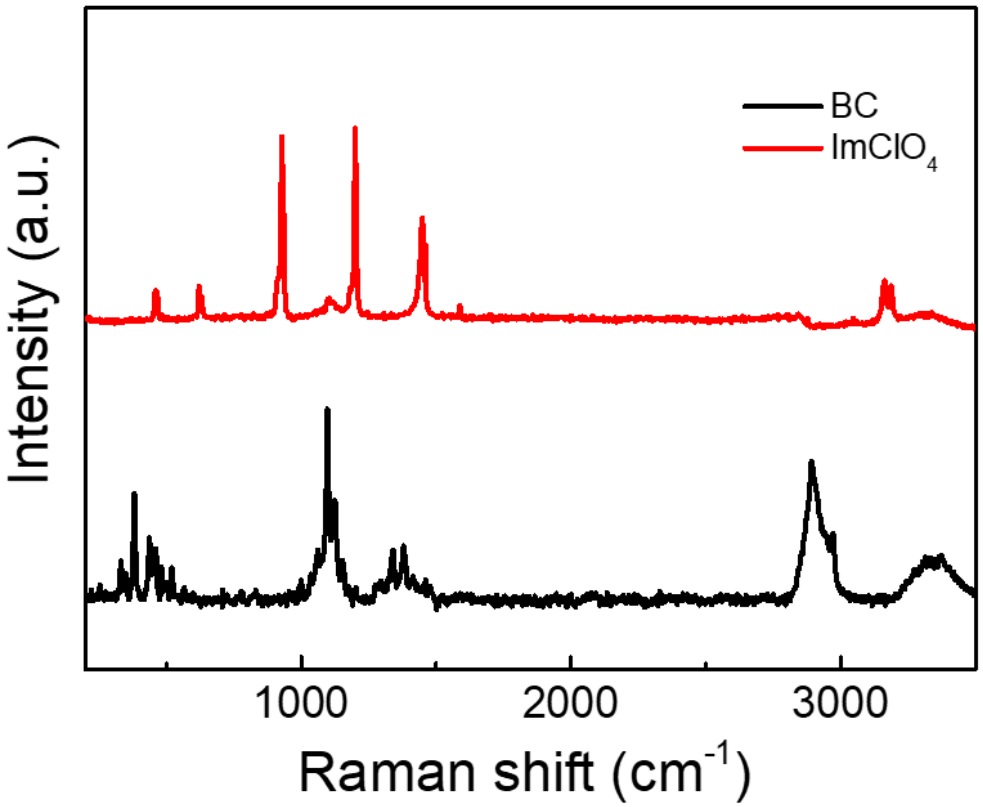

Figure S1. The Raman spectra of the BC membrane and the $ImClO_4$ crystal.

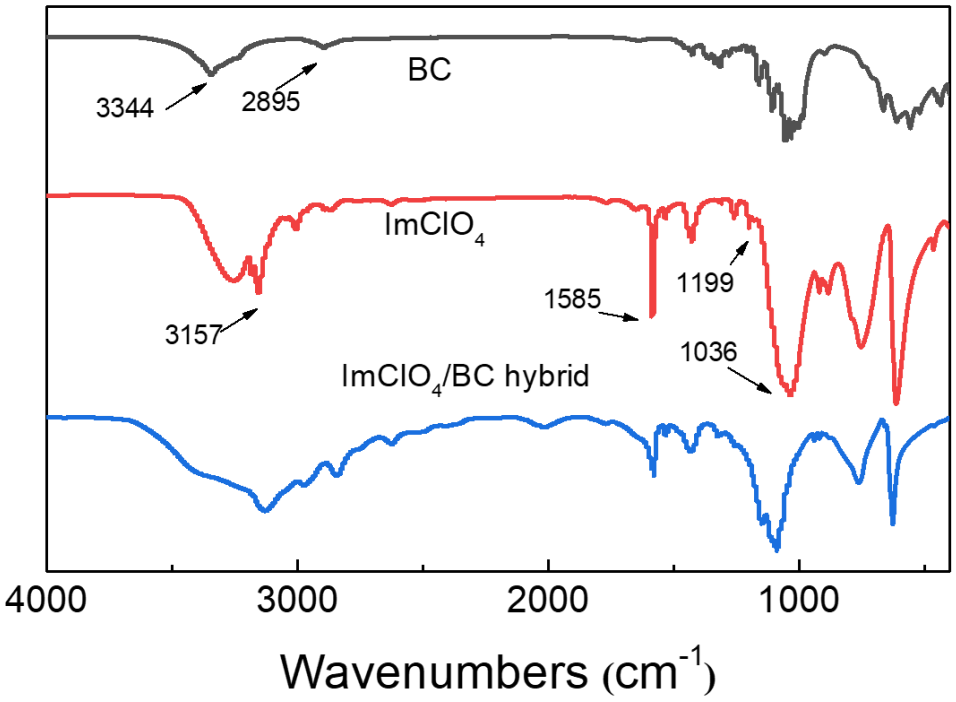

Figure S2. The FTIR spectra of the BC membrane, the $ImClO_4$ crystal and $ImClO_4$/BC hybrid.

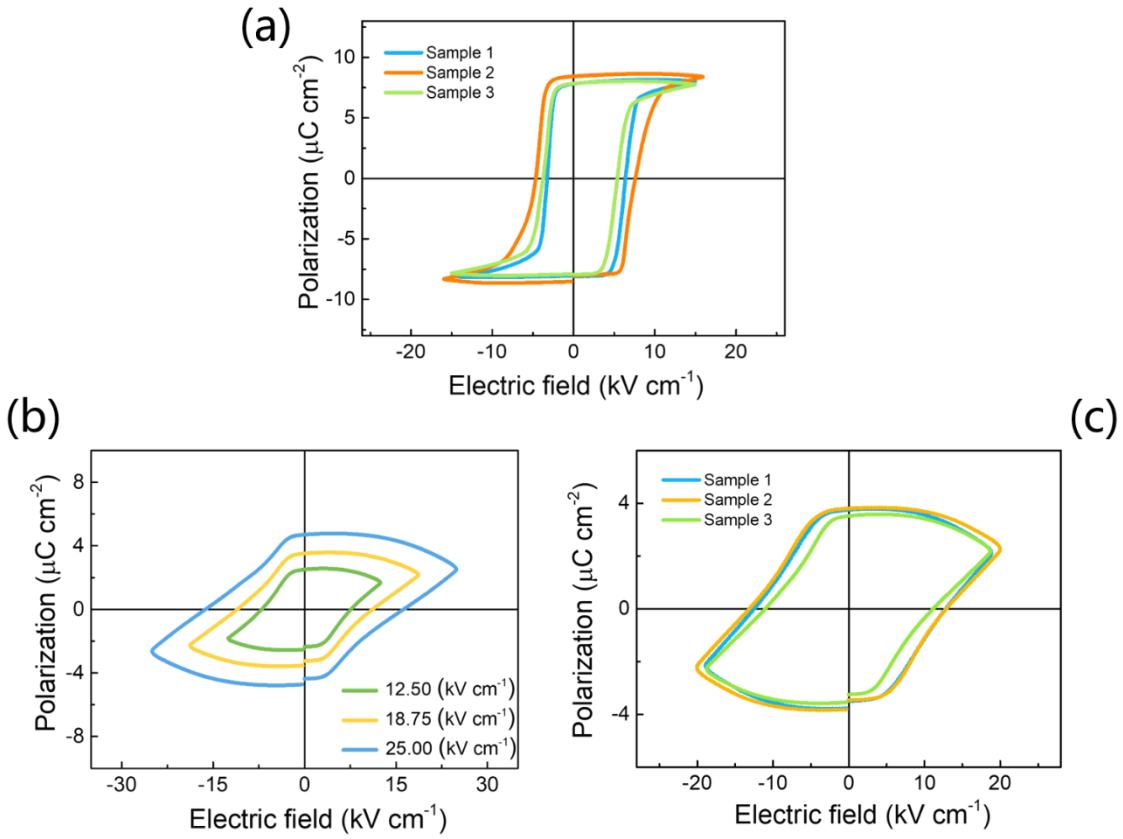

Figure S3. (a) The polarization-electric field (*P*-*E*) hysteresis loops of the $ImClO_4$ crystal (We tested 3 samples to confirm the uniformity of the crystals). (b) The *P*-*E* loops of the molecular ferroelectric/BC hybrid with various electric fields. (c) The *P*-*E* loops of 3 hybrid specimens were tested to confirm the uniformity of the hybrid strategy.

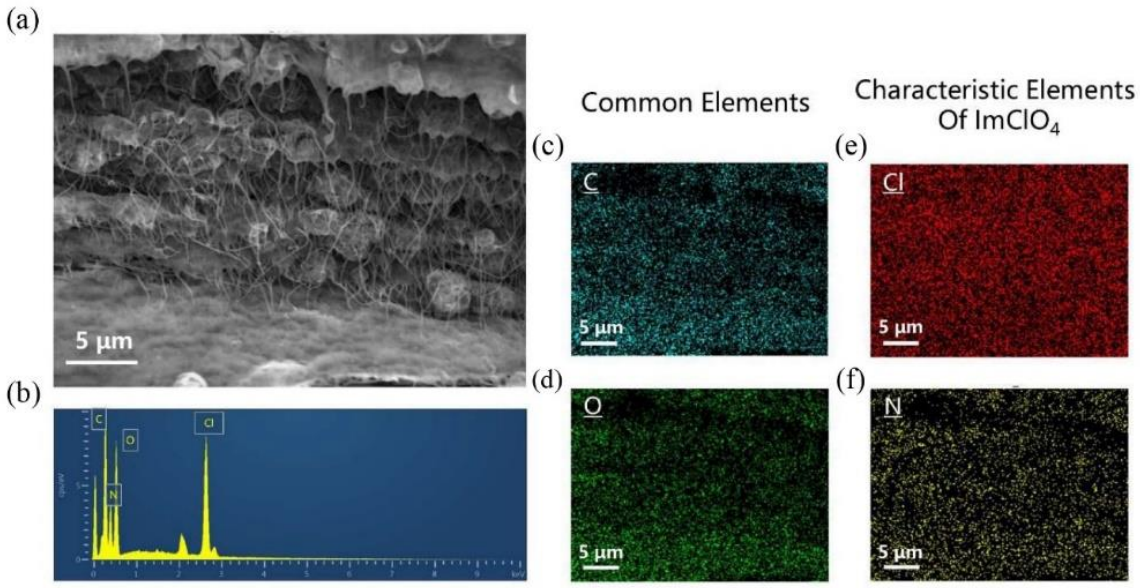

Figure S4. The EDS (a) image, (b) spectrum, and (c-f) mappings of the hybrid. C and O are the common elements for BC membrane and $ImClO_4$, and Cl and N are characteristic elements for $ImClO_4$.

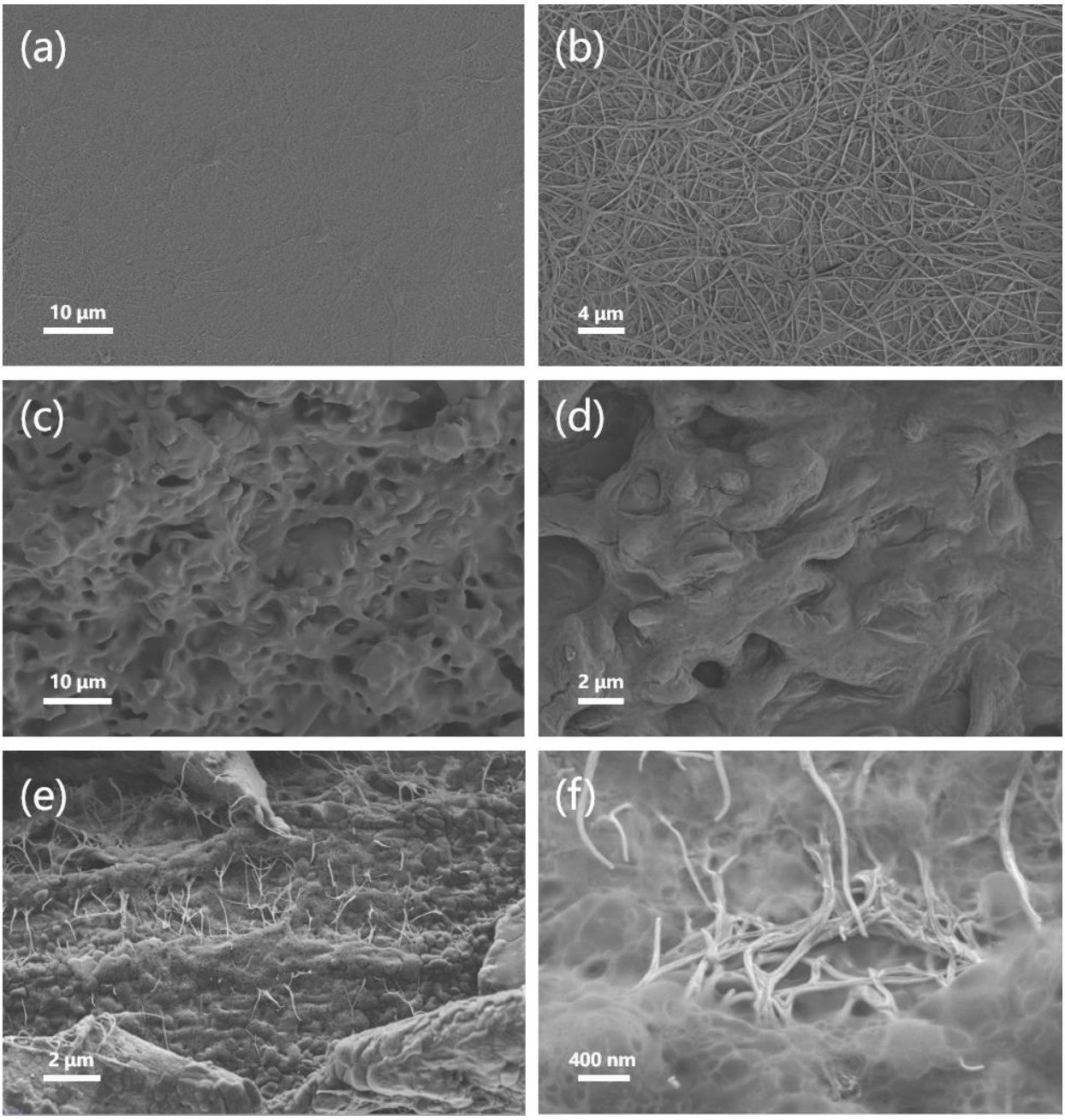

Figure S5. The SEM images of (a) and (b) the surface of the BC membrane, (c) and (d) $ImClO_4$/BC hybrid. (e) and (f) the cross-section view of the hybrid.

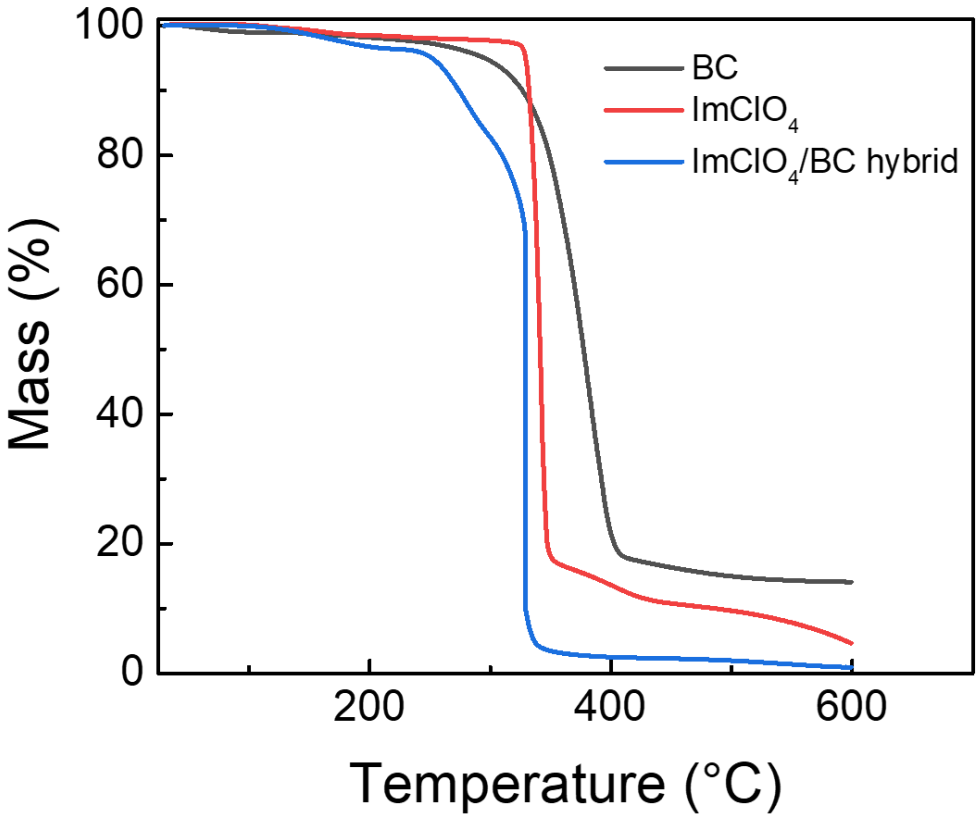

Figure S6. The TGA curves of BC membrane, $ImClO_4$ crystal and $ImClO_4$/BC hybrid.

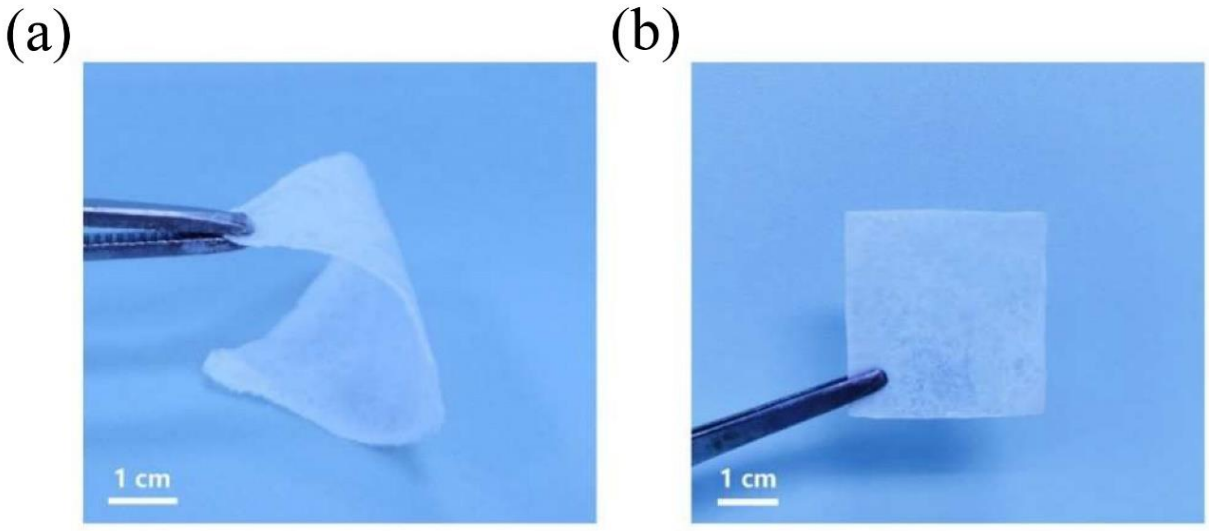

Figure S7. The optical images of a flexible molecular ferroelectric/BC hybrid.

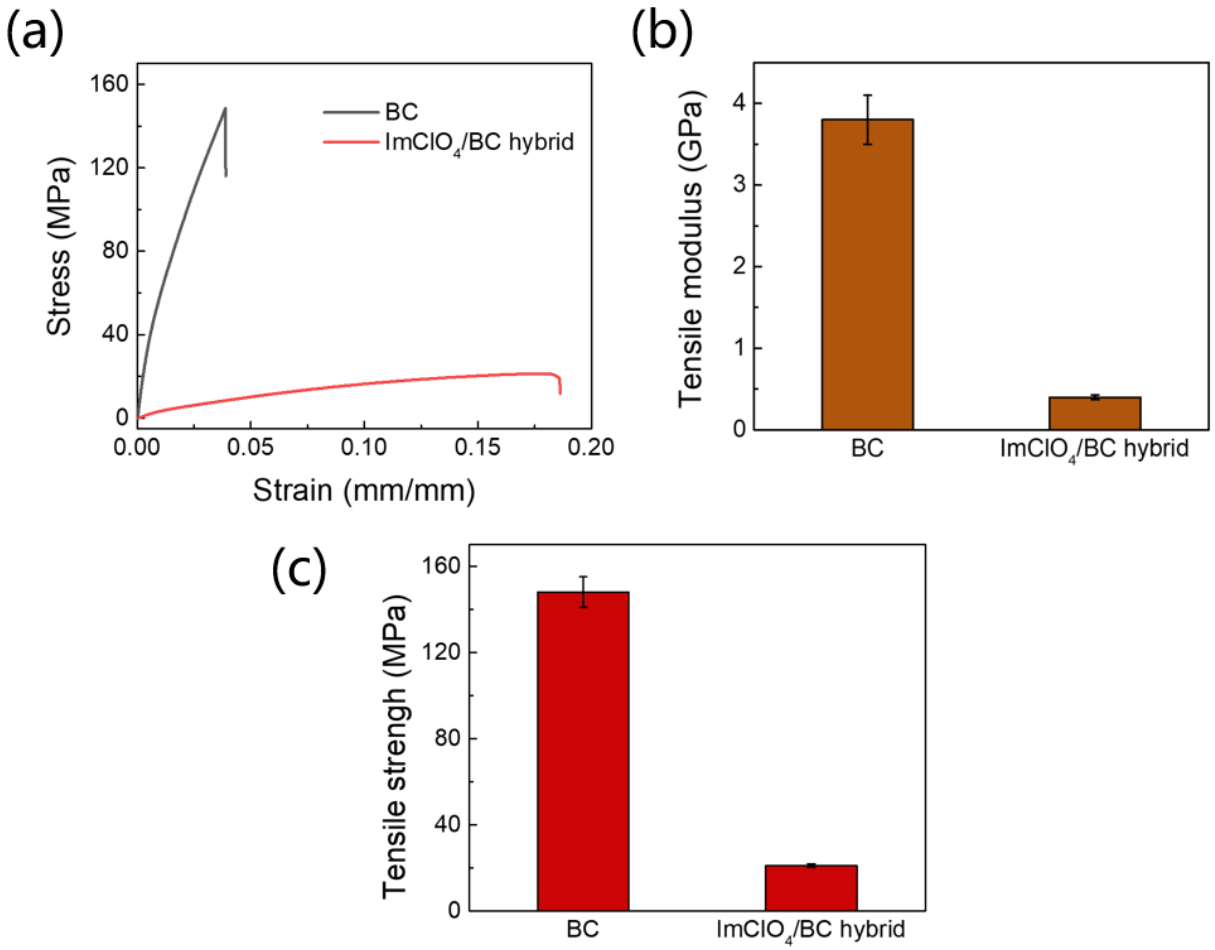

Figure S8. The mechanical properties of BC membrane and $ImClO_4$/BC hybrid. (a) The stress-strain curves of the samples. (b) and (c) The tensile modulus and tensile strength of the specimens.

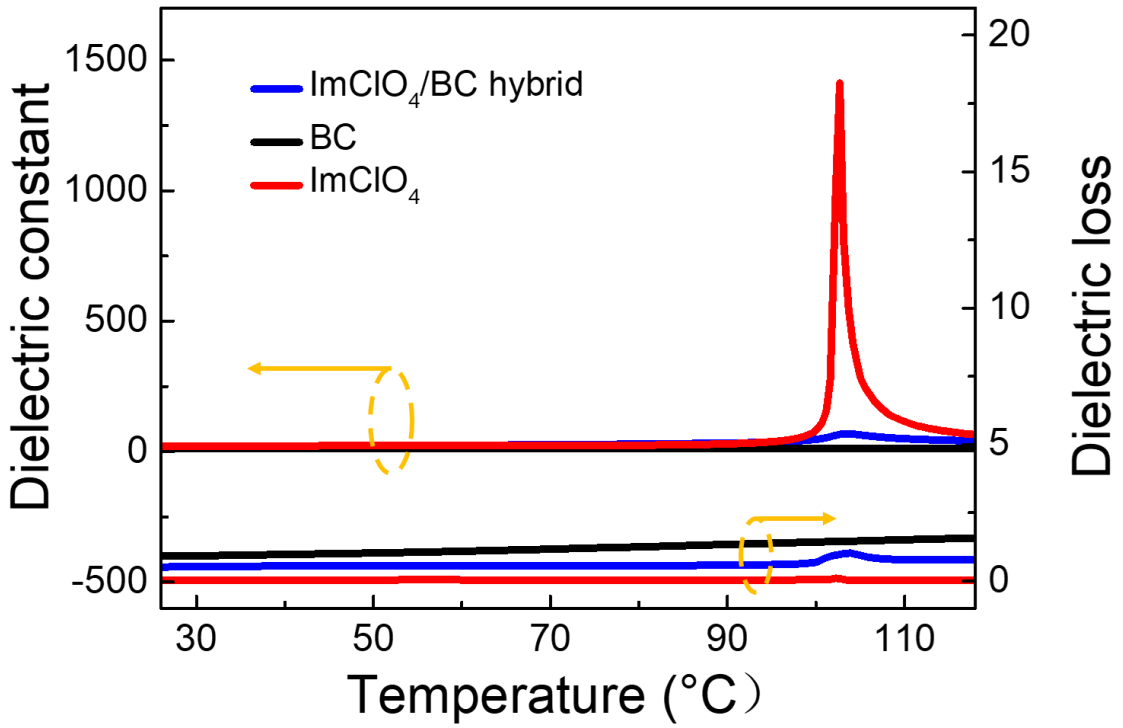

Figure S9. The dielectric constant and loss as a function of temperature of BC membrane, $ImClO_4$ crystal and $ImClO_4$/BC hybrid.

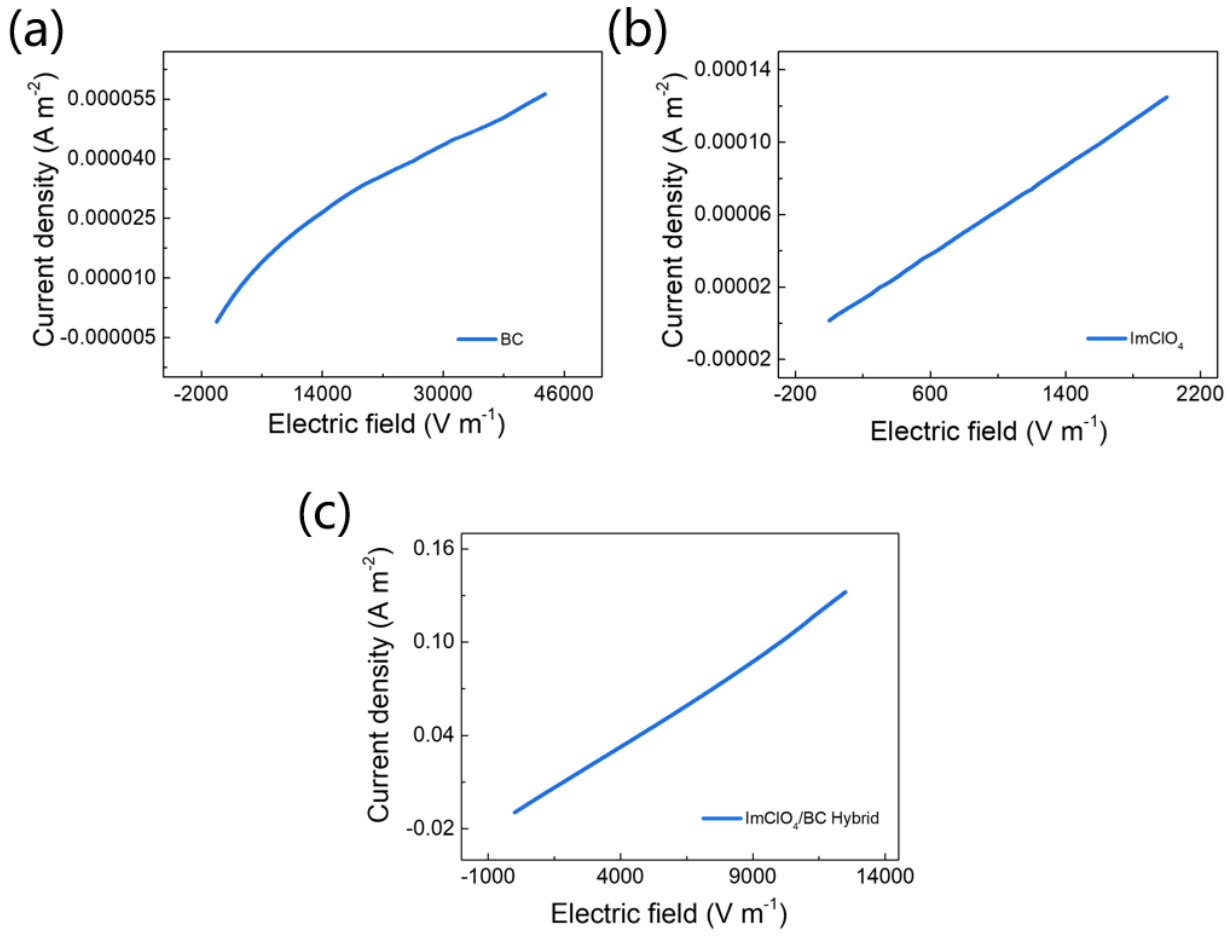

Figure S10. The current density-electric field curves of BC membrane, $ImClO_4$ crystal and $ImClO_4$/BC hybrid.

Table S2. The piezoelectric voltage of 16 samples with various pressures.

Voltage (mV) / Pressure (kPa)	Sample Number																Mean	S.D.
	1	**2**	**3**	**4**	**5**	**6**	**7**	**8**	**9**	**10**	**11**	**12**	**13**	**14**	**15**	**16**		
0.20	3.70	5.28	3.62	4.50	4.18	4.35	4.45	5.24	4.73	6.10	4.92	4.08	4.26	4.25	3.87	3.70	4.45	0.67
1.25	8.47	11.58	8.10	8.47	8.10	9.32	9.40	9.35	9.44	10.08	9.04	9.61	11.40	10.11	10.75	8.47	9.51	1.05
2.50	15.80	16.38	15.96	15.58	17.67	17.41	16.38	17.28	17.40	16.86	13.92	17.72	22.66	15.82	17.00	15.80	16.93	1.81
3.75	19.51	22.93	20.97	19.37	23.03	18.47	18.58	20.72	22.79	20.15	21.94	22.66	22.93	21.94	22.66	19.51	21.28	1.62
5.00	20.17	23.62	22.76	22.46	23.13	19.27	19.77	22.81	23.03	21.99	24.37	23.74	23.56	23.80	23.42	20.17	22.58	1.53
6.25	27.50	31.64	27.17	27.58	25.49	27.50	27.05	29.83	26.80	27.97	26.71	27.73	26.41	28.48	28.68	27.50	27.73	1.44
7.50	39.20	41.65	36.32	35.59	41.10	41.85	38.62	38.89	37.85	39.03	39.96	40.95	41.48	39.12	23.42	39.20	39.46	1.82

Note: S.D. is standard deviation.

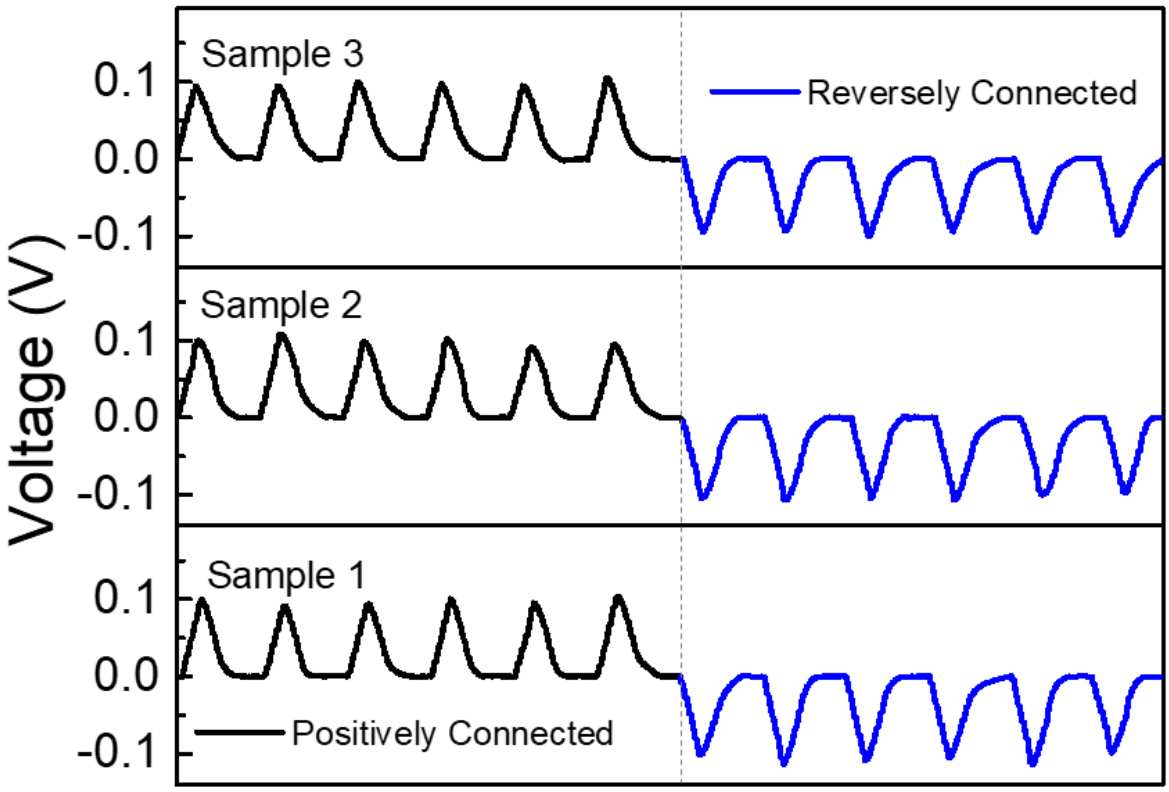

Figure S11. The piezoelectric voltage waveforms of the $ImClO_4$/BC hybrid. The positive response when the sensor is positively connected matches well with the negative signal as it is reversely connected (25 kPa). We tested 3 samples to confirm the uniformity and scalability of our strategy.

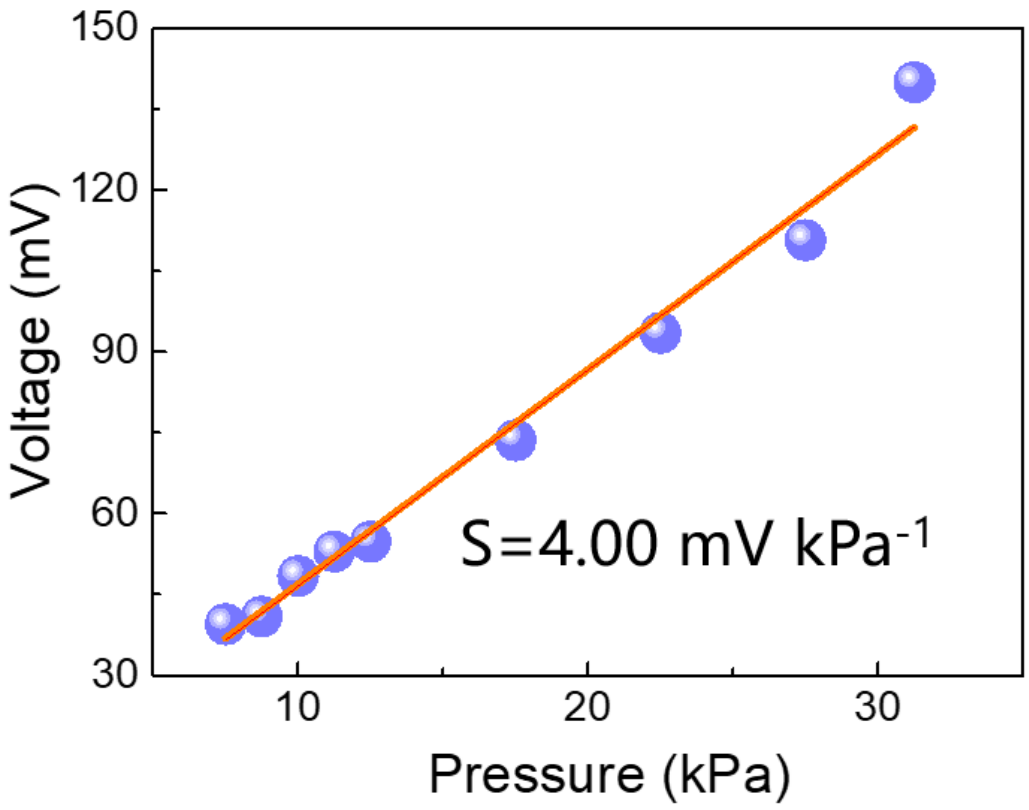

Figure S12. The piezoelectric response of the hybrid sensor with various pressures (8 kPa-31.25 kPa). The sensitivity of the sensor (*i.e.* slope of linear fitting of the plots) is 4 mV kPa^{-1}.

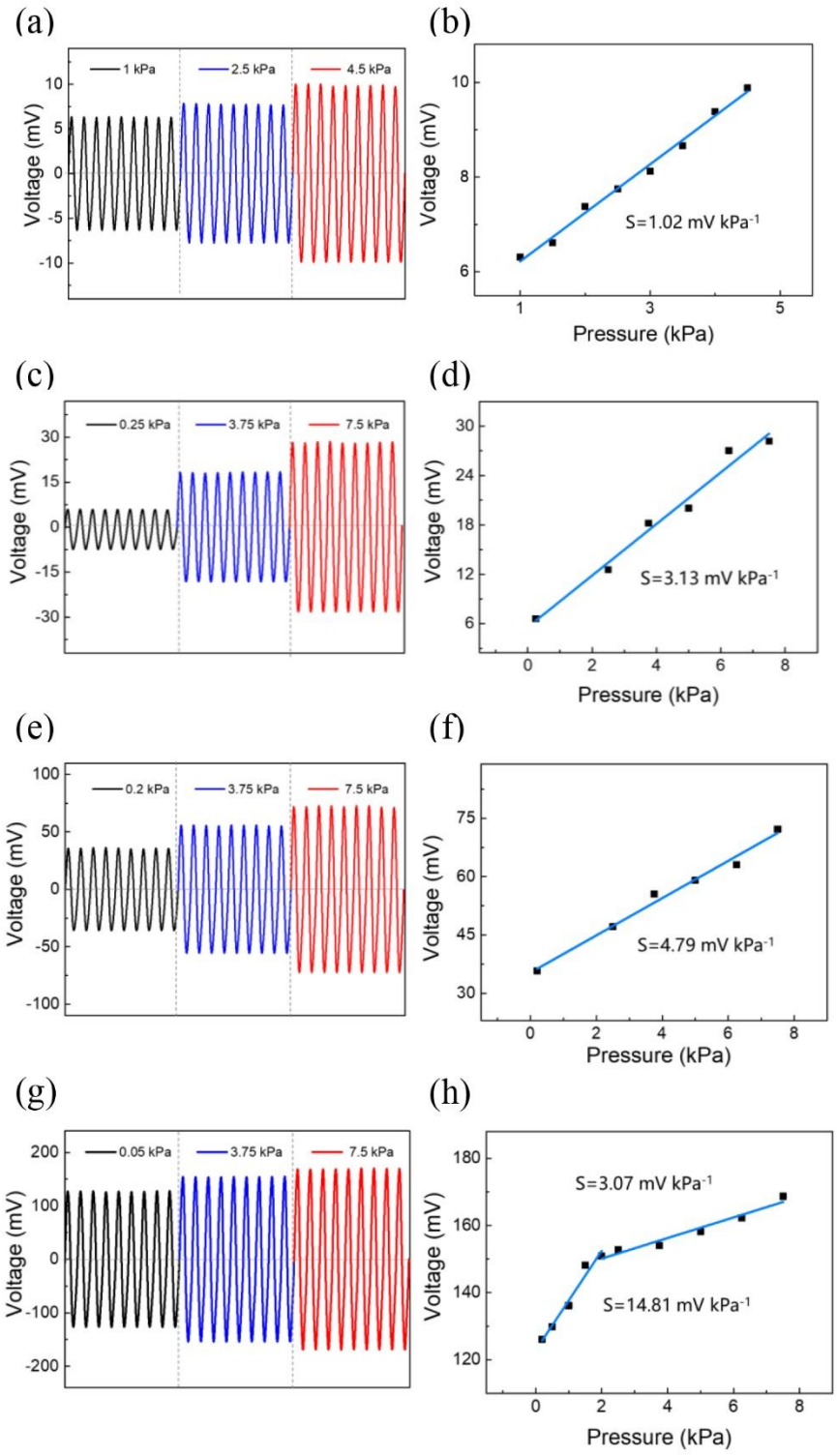

Figure S13. The piezoelectric voltage response and sensitivity of $ImClO_4$/BC hybrid with various thicknesses: (a,b) 65 μm, (c,d) 130 μm, (e,f) 220 μm and (g,h) 370 μm.

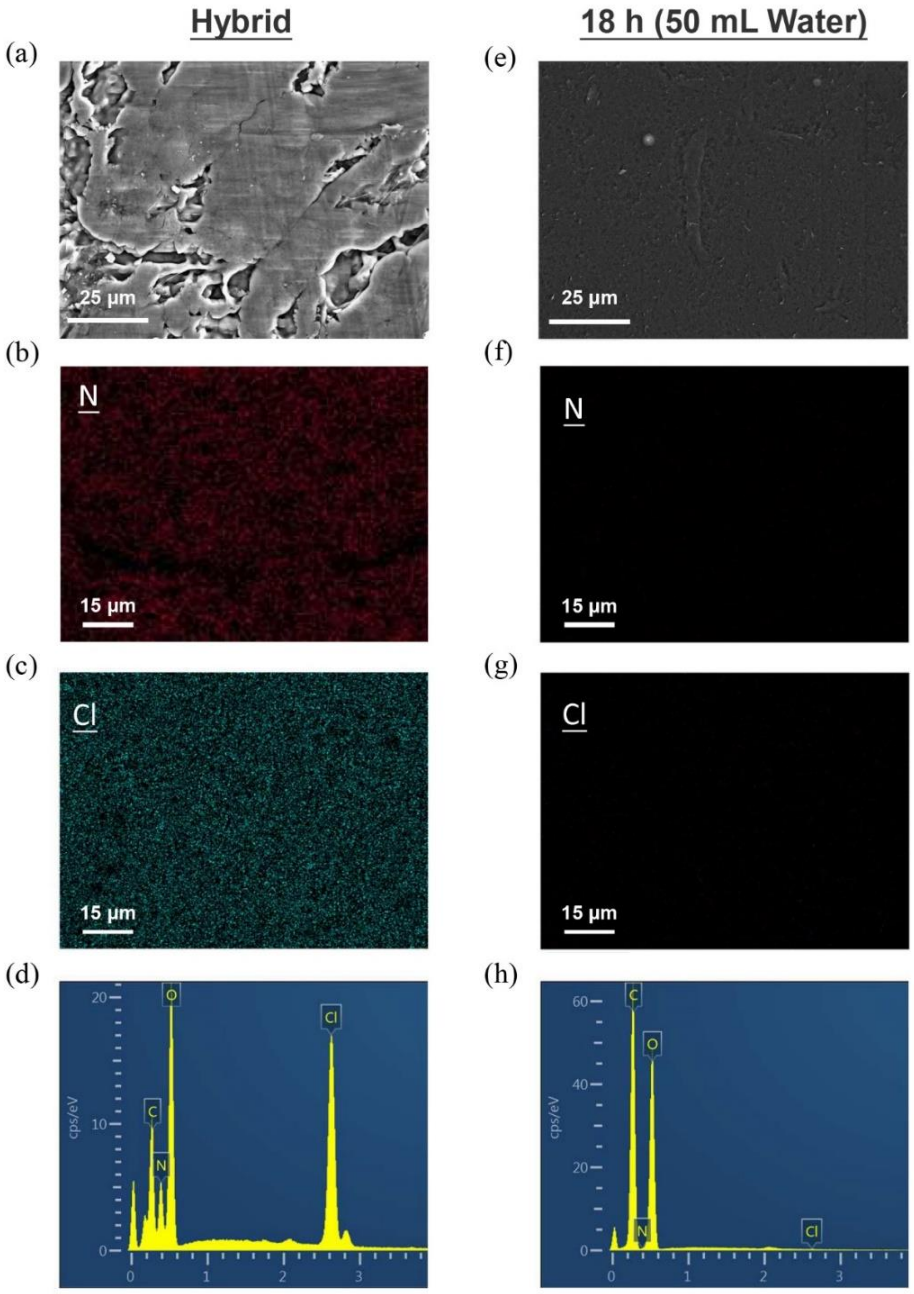

Figure S14. The EDS images, mappings and spectrum of the characteristic elements of $ImClO_4$ (nitrogen and chlorine) of the hybrid [(a), (b), (c), (d), respectively] and that after soaking in 50 mL water for 18 h [(e), (f), (g), (h), respectively], proving the feasibility of separating the molecular ferroelectric and the BC membrane.

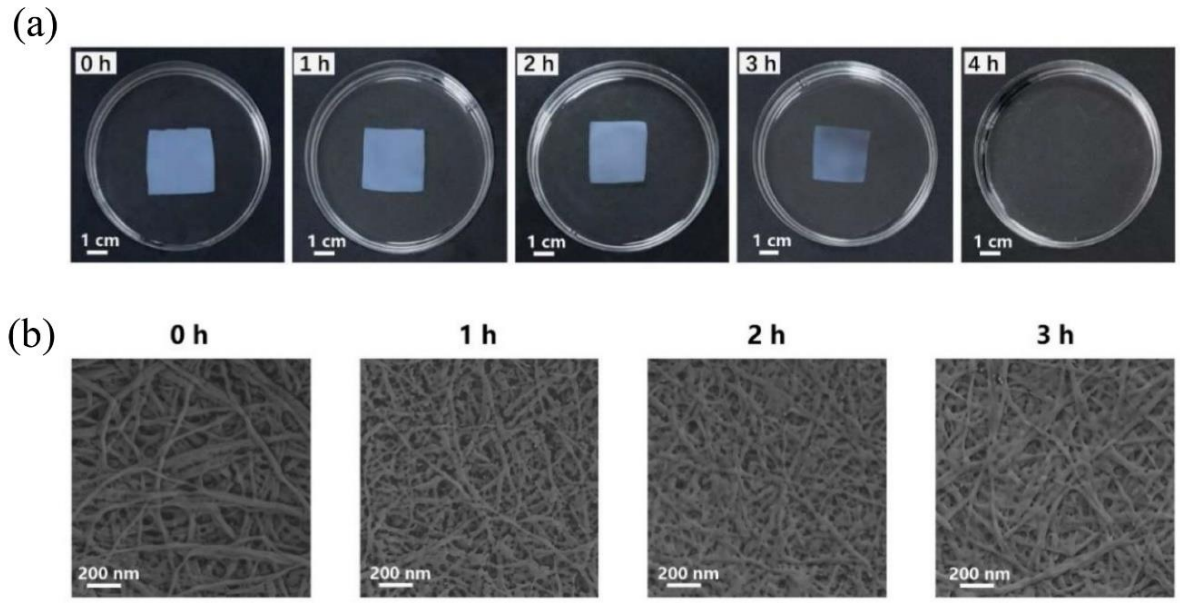

Figure S15. (a) Optical and (b) SEM images illustrating the degradation process of a brand-new BC membrane. The membrane can be fully degraded within 4 h in a cellulase solution (5 mg mL^{-1}, 50 ^{o}C).

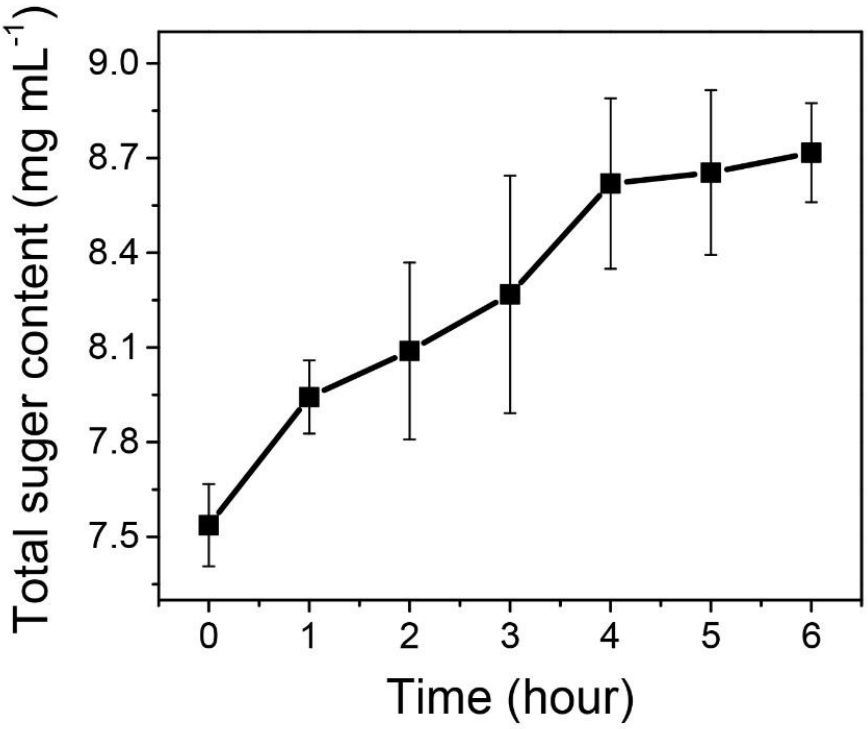

Figure S16. The curve of total sugar concentration during the degradation process of the recycled BC membrane (error bar: standard deviation). The BC membrane can be fully degraded within 4 h in a cellulase solution (5 mg mL^{-1}, 50 ^{o}C).

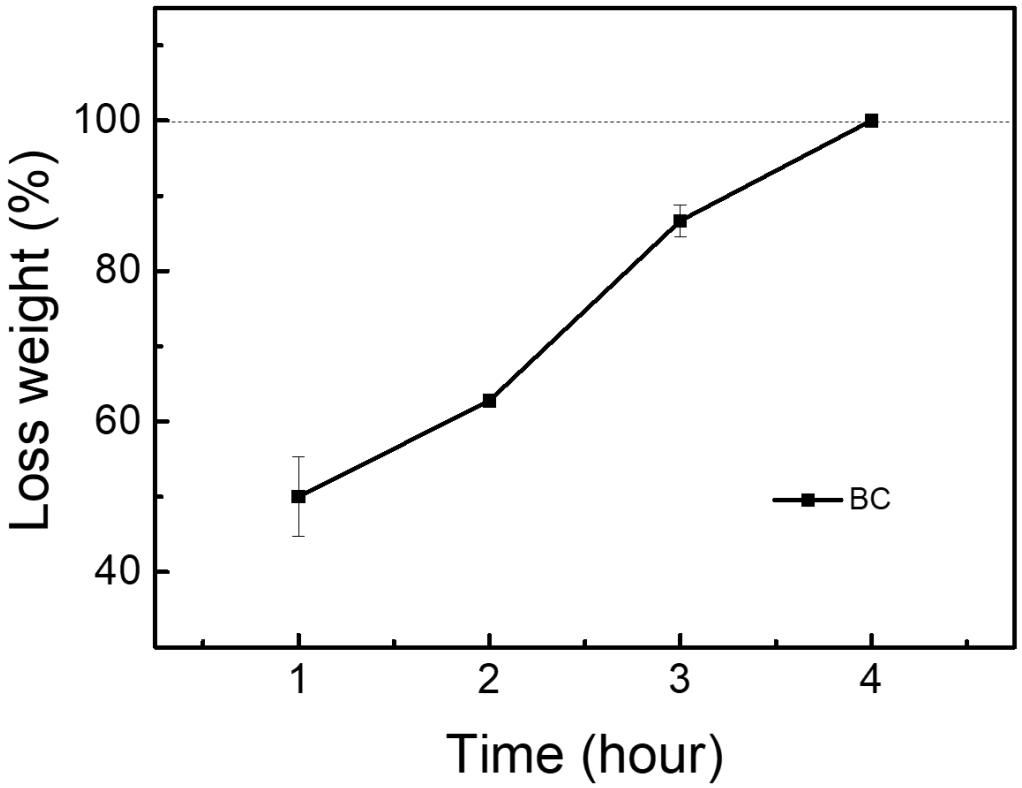

Figure S17. The weight loss of a recycled BC membrane having been immersed in the cellulase solution with different time.

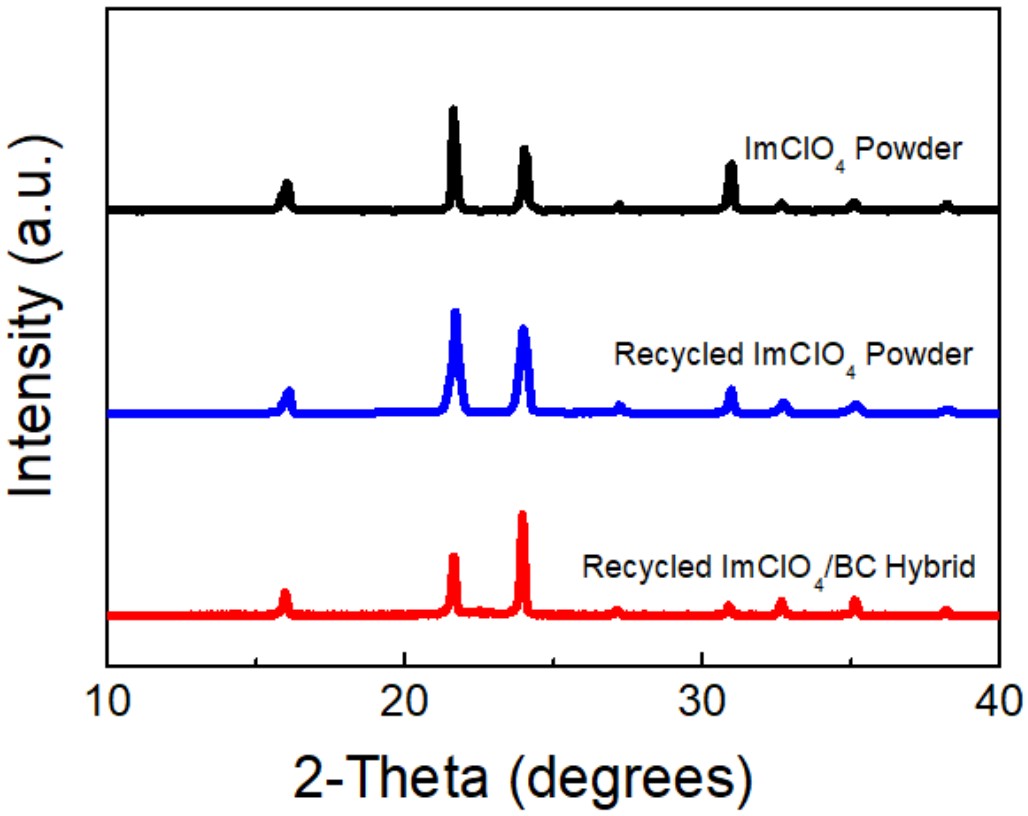

Figure S18. The XRD pattern of original and recycled $ImClO_4$ powders, and the hybrid prepared with the recycled $ImClO_4$.

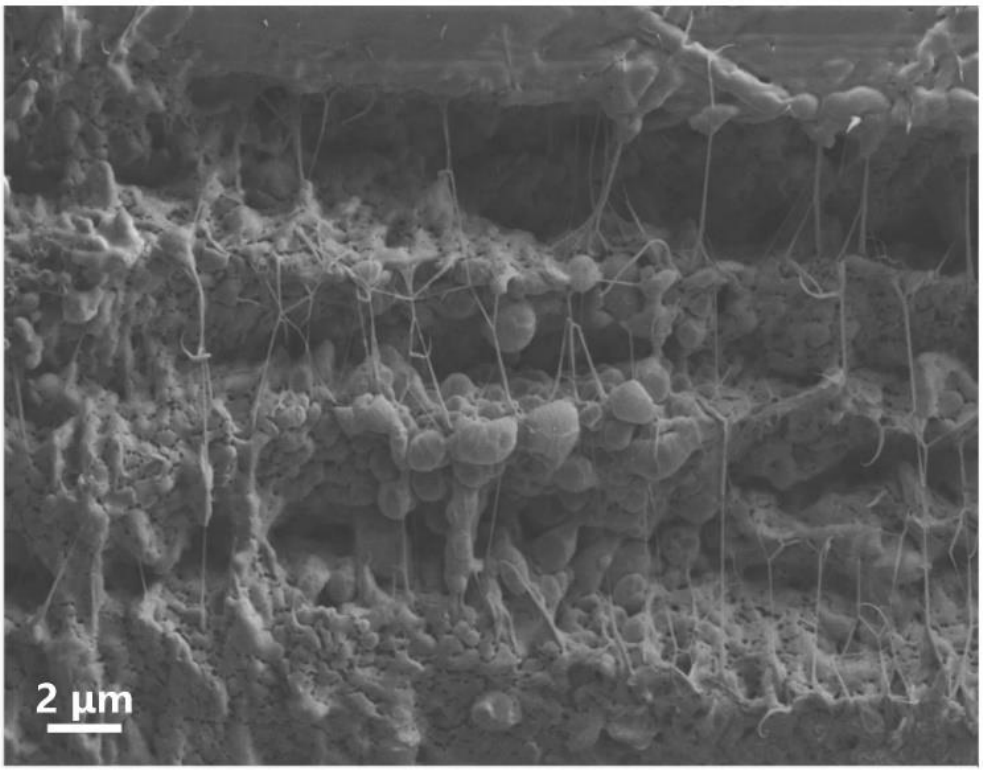

Figure S19. The cross-section SEM image of a recycled molecular ferroelectric/BC hybrid.

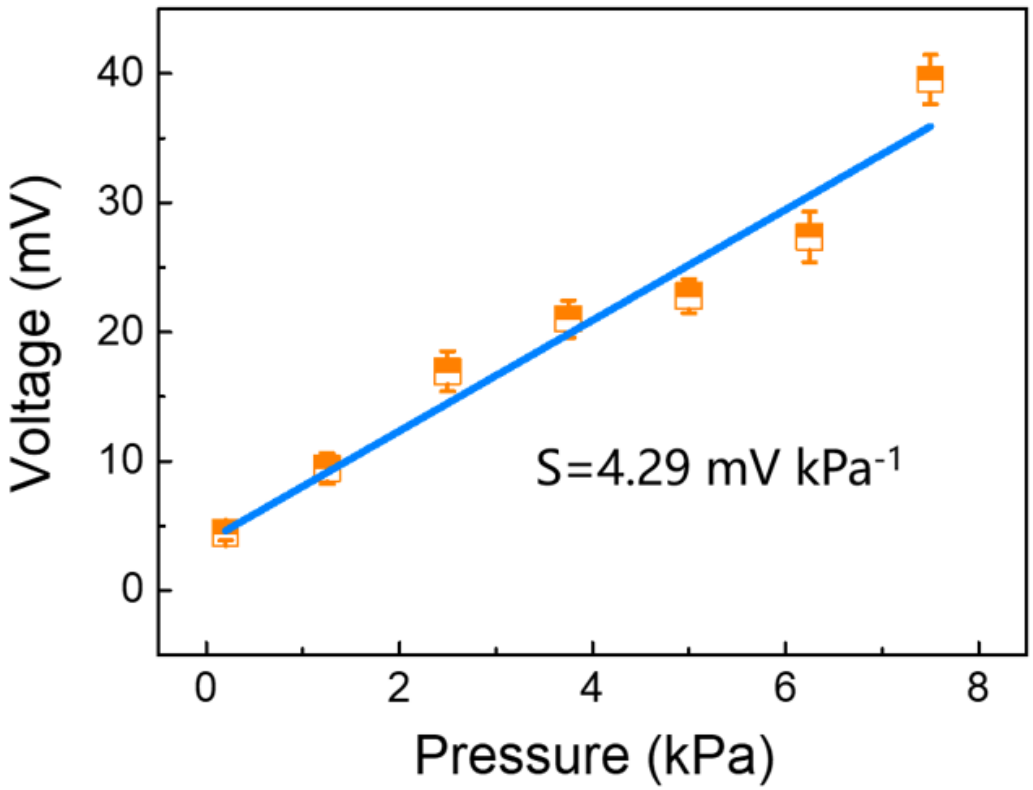

Figure S20. Sensor response as a function of applied pressure (error bar: standard deviation, Table S3, Supporting Information) with the slope (sensitivity) of 4.29 mV kPa^{-1}.

Table S3. The piezoelectric voltage of 16 recycled samples with various pressures.

Voltage (mV) / Pressure (kPa)	Sample Number																Mean	S.D.
	1	**2**	**3**	**4**	**5**	**6**	**7**	**8**	**9**	**10**	**11**	**12**	**13**	**14**	**15**	**16**		
0.20	4.01	3.53	3.62	4.63	4.56	4.72	4.12	5.08	4.62	5.25	4.78	5.47	4.70	3.81	4.35	3.81	4.44	0.58
1.25	8.52	8.47	8.57	10.63	9.48	8.90	8.65	11.65	9.35	9.37	10.92	10.50	11.27	7.29	8.47	8.90	9.43	1.22
2.50	16.80	14.77	15.08	19.03	17.24	17.43	14.69	19.10	17.64	14.98	17.85	19.27	15.33	17.41	17.41	17.24	16.95	1.56
3.75	21.19	18.98	18.06	21.41	21.94	20.84	22.66	22.79	22.93	19.06	21.96	21.60	20.52	20.29	19.81	21.94	20.99	1.45
5.00	22.86	19.27	21.87	22.76	22.48	20.32	23.89	23.96	24.42	22.06	22.89	24.09	22.94	21.90	21.94	22.82	22.65	1.22
6.25	26.51	25.03	26.32	28.69	27.50	28.50	26.33	32.01	30.37	24.62	26.22	26.25	29.21	27.17	25.95	27.17	27.36	1.96
7.50	38.63	38.90	37.21	40.90	40.47	40.90	38.90	38.95	39.13	41.67	39.09	42.04	39.29	34.97	39.67	40.47	39.45	1.73

Note: S.D. is standard deviation

REFERENCES

S1. Liao, W. Q.; Zhao, D. W.; Tang, Y. Y.; Zhang, Y.; Li, P. F.; Shi, P. P.; Chen, X. G.; You, Y. M.; Xiong, R. G. A Molecular Perovskite Solid Solution with Piezoelectricity Stronger Than Lead Zirconate Titanate. *Science* **2019**, *363*, 1206-1210. DOI: 10.1126/science.aav3057

S2. Fu, D. W.; Cai, H. L.; Liu, Y. M.; Ye, Q.; Zhang, W.; Zhang, Y.; Chen, X. Y.; Giovannetti, G.; Capone, M.; Li, J. Y.; Xiong, R. G. Diisopropylammonium Bromide Is a High-Temperature Molecular Ferroelectric Crystal. *Science* **2013**, *339*, 425-428. DOI: 10.1126/science.1229675

S3. Pan, Q.; Liu, Z. B.; Zhang, H. Y.; Zhang, W. Y.; Tang, Y. Y.; You, Y. M.; Li, P. F.; Liao, W. Q.; Shi, P. P.; Ma, R. W.; Wei, R. Y.; Xiong, R. G. A Molecular Polycrystalline Ferroelectric with Record-High Phase Transition Temperature. *Adv. Mater.* **2017**, *29*, 1700831. DOI: 10.1002/adma.201700831

S4. Zhang, Y.; Ye, H. Y.; Cai, H. L.; Fu, D. W.; Ye, Q.; Zhang, W.; Zhou, Q. H.; Wang, J. L.; Yuan, G. L.; Xiong, R. G. Switchable Dielectric, Piezoelectric, and Second-Harmonic Generation Bistability in a New Improper Ferroelectric above Room Temperature. *Adv. Mater.* **2014**, *26*, 4515-4520. DOI: 10.1002/adma.201400806

S5. Mu, X.; Xu, L.; Xu, Y. Y.; Zhang, H. Y.; Xiong, R. G. High-Temperature Enantiomeric Azobenzene-Based Photoisomerized Piezoelectrics: 4-(Phenyldiazenyl)Anilinium) D- and L-Tartrate. *Mater. Chem. Front.* **2021**, *5*, 8371-8379. DOI: 10.1039/D1QM01157J

S6. Chen, X. G.; Song, X. J.; Zhang, Z. X.; Li, P. F.; Ge, J. Z.; Tang, Y. Y.; Gao, J. X.; Zhang, W. Y.; Fu, D. W.; You, Y. M.; Xiong, R. G. Two-Dimensional Layered Perovskite Ferroelectric with Giant Piezoelectric Voltage Coefficient. *J. Am. Chem. Soc.* **2020**, *142*, 1077-1082. DOI: 10.1021/jacs.9b12368

S7. Ye, H. Y.; Tang, Y. Y.; Li, P. F.; Liao, W. Q.; Gao, J. X.; Hua, X. N.; Cai, H.; Shi, P. P.; You, Y. M.; Xiong, R. G. Metal-Free Three-Dimensional Perovskite Ferroelectrics. *Science* **2018**, *361*, 151-155. DOI: 10.1126/science.aas9330

S8. Wang, Z. X.; Zhang, H.; Wang, F.; Cheng, H.; He, W. H.; Liu, Y. H.; Huang, X. Q.; Li, P. F. Superior Transverse Piezoelectricity in a Halide Perovskite Molecular Ferroelectric Thin Film. *J. Am. Chem. Soc.* **2020**, *142*, 12857-12864. DOI: 10.1021/jacs.0c06064

S9. You, Y. M.; Liao, W. Q.; Zhao, D. W.; Ye, H. Y.; Zhang, Y.; Zhou, Q. H.; Niu, X. H.; Wang, J. L.; Li, P. F.; Fu, D. W.; Wang, Z. M.; Gao, S.; Yang, K. L.; Liu, J. M.; Li, J. Y.; Yan, Y. F.; Xiong, R. G. An Organic-Inorganic Perovskite Ferroelectric with Large Piezoelectric Response. *Science* **2017**, *357*, 306-309. DOI: 10.1126/science.aai8535